Eur. Phys. J. B **53**, 323–331 (2006)
DOI: 10.1140/epjb/e2006-00387-2

THE EUROPEAN PHYSICAL JOURNAL B

Comparative study of magnetic and electric field induced insulator-metal-transitions in $Pr_{1-x}Ca_xMnO_3$ films

W. Westhäuser, S. Schramm, J. Hoffmann, and C. Jooss[a]

Institut für Materialphysik, Friedrich-Hund-Platz 1, 37077 Göttingen, Germany

Received 6 June 2006 / Received in final form 8 September 2006
Published online 20 October 2006 –

Abstract. The insulator-metal (IM)-transition in $Pr_{1-x}Ca_xMnO_3$ (PCMO) is of particular interest because it can be induced by a variety of external forces, such as magnetic and electric fields, photon exposure and hydrostatic pressure. In this paper, we present a comparative study of the IM-transition in magnetic and electric fields for epitaxial thin films prepared by pulsed laser deposition. The transport data as a function of applied field or temperature give strong evidence for the presence of electronic phase separation. However, the observed different IM-transitions in magnetic and electric fields indicate that two different areas of spatially inhomogeneous electronic ground states in the phase diagram of PCMO are involved.

PACS. 73.50.-h Electronic transport phenomena in thin films – 75.47.-m Magnetotransport phenomena; materials for magnetotransport – 75.47.Lx Manganites – 71.30.+h Metal-insulator transitions and other electronic transitions

1 Introduction

The compound $Pr_{1-x}Ca_xMnO_3$ is a representative of the material class of hole-doped manganites, in which a phase transition from an insulating to a conducting state (IM-transition) can be induced by external forces, like magnetic fields (CMR) [1–6], electric fields [7–11], hydrostatic pressure [12], and photon exposure [13–19]. The temperature vs. Ca-doping phase diagrams proposed by Jirak et al. [20], Tonogai et al. [21] and Hill et al. [22] reveal a series of insulating ground states in the doping range between $0.0 \leq x \leq 0.7$. At the phase boundary of $x = 0.3$, a ferromagnetic insulating (FI) ground state ($T_C \approx 130$ K) is suggested to transform into an orbital ordered (OO) state with CE-type antiferromagnetic (AFM) spin ordering ($T_N \approx 140$ K) and a possibly canted antiferromagnetic state (CAFI) below $T_{CA} \approx 110$ K, respectively. It is widely believed [20,21,23] that also charge ordering (CO) is present in the doping range $0.3 \leq x \leq 0.7$ with an ordering temperature T_{CO} of about 230 K. According to [23], the onset of charge ordering at T_{CO} is directly correlated to the development of orbital ordering. Both types of ordering give rise to a highly insulating state, which can be destabilized by applying an external force. At a critical value of the force, disordering of the OO/CO takes place, resulting in an insulator-metal-transition with the emergence of a low-resistivity phase. In the case of CO, the IM-transition is often pictured as a transition from a charge-crystal with Mn^{3+}–Mn^{4+} valence state positional ordering to a charge-liquid of delocalized charge carriers, in which the charge transport may be governed by mobile polarons or electrons [24,25].

Recently, considerable controversies have been developed on the nature and also on the presence of Mn charge disproportionation. Based on neutron diffraction data, Daoud-Aladine et al. [26] suggest ordering of Zener polarons, where the charge disproportionation between different Mn sites is less than 0.1 electron charge. This is supported by further theoretical work [27,28] and a recent study on BiCaMnO [29], which suggests that CO is in fact *orbital occupancy* ordering, where all Mn atoms possesses the same physical charge. In contrast to orbital ordering which can be uniquely proven by the occurrence of superlattice reflections (related to the corresponding displacements of the oxygen atoms), the presence of charge ordering therefore is considered as unclear. Mentioning in the following an OO/CO state, this refers to the usual nomenclature of the low temperature phase at $0.3 \leq x \leq 0.7$ without claiming that CO is proven.

Indeed, we expect the orbital ordering as one crucial factor of the IM-transition, because the onset of polaron mobility is related to a disordering of the cooperative static Jahn Teller distortions. This is strongly supported by our experiments on the long-term relaxation of the resistivity.

In addition, as suggested by various theoretical work [30–34], electronic phase separation seems to play an important role in the IM-transition. In this model, depending on the temperature and the doping, the ground

[a] e-mail: jooss@ump.gwdg.de

Table 1. Lattice parameters of the PLD films on $SrTiO_3$ (STO) and MgO (001) substrates before and after annealing. Due to twinning and small orthorhombicity, a and b are not distinguished for the films. The single crystalline values for $x = 0.3$ are taken from reference [20].

Sample	type	a or b[nm]	c [nm]	
A	STO as prepared	0.541 ± 0.002	0.772 ± 0.003	
B	STO annealed	0.543 ± 0.002	0.767 ± 0.003	
C	MgO as prepared	0.543 ± 0.002	0.774 ± 0.002	
D	MgO annealed	0.542 ± 0.002	0.775 ± 0.002	
		a [nm]	b[nm]	c [nm]
Single crystal		0.5426	0.5478	0.7679

state of the chemically homogeneous crystal is expected to be composed of conducting and insulating phases. External forces may increase the volume fraction of the conducting phase, i.e. the transition to a low-resistivity state takes place above the percolation threshold [35]. An electronic phase separation has been indeed observed for manganites with a ferromagnetic conducting ground state, e.g. $La_{1-x}Ca_xMnO_3$ and $La_{1-x}Sr_xMnO_3$. During the temperature-induced insulator-metal-transition, nanometer sized conducting electronic domains were observed by STM measurements [36,37]. For the $Pr_{1-x}Ca_xMnO_3$ system, up to now, there is no direct proof of an electronic phase separation. However, large electronic domains were imaged by transmission electron microscopy in the system $(La,Pr)_{1-x}Ca_xMnO_3$ [38]. Furthermore, in $Pr_{1-x}Ca_xMnO_3$, photon exposure induces a strongly localized IM-transition, related to the formation of conductive filaments [16–18].

With respect to a possible phase separation in $Pr_{1-x}Ca_xMnO_3$, the doping-concentration of $x \approx 0.30$ (in the following indicated as PCMO) is of particular interest, because at this phase boundary, the low temperature insulating ferromagnetic state coexists with an OO/CO state [21]. In this doping induced phase transformation, at least, the ordering of two different degrees of freedom are involved, spin and orbital. However, similar to the unsolved questions of CO, neither the detailed structure of OO nor the type of magnetic ordering is well understood. Instead of the CAFI state suggested by reference [21], the presence of small ferromagnetic (FM) clusters embedded in an AFM environment was already suggested by Jirak et al. [20]. Several authors [30–34] discuss a similar picture. In general, it is observed that at doping levels of $x \approx 0.30$ the ground state seems to be most sensitive to the magnetic field-induced phase transition (CMR) [39].

In this contribution, we concentrate on the striking differences of the resistivity behaviour in magnetic and electric fields. Both kind of field-induced transitions are strongly hysteretic and changes the resistivity by orders of magnitude, however, the shape of the temperature dependence as well as the characteristic temperature are quite different. To our knowledge, up to now, the published results either reporting on transport properties of $Pr_{1-x}Ca_xMnO_3$ in magnetic [1–6] or in electric fields [7–11]. To exclude a possible influence of small preparation-caused microstructural or chemical differences, our measurements were performed on the same samples. The results concerning the temperature-dependent resistivity and its relaxation in both, electric and magnetic field, are discussed with respect to the controversial issues of the role of CO/OO and a possible presence of electronic phase separation in the IM-transition of PCMO.

2 Experimental details

All experiments presented in this article are performed on high-quality epitaxial PCMO films. The films with a thickness of 250 nm are grown by pulsed laser deposition (PLD). The polycrystalline ceramic targets were prepared by a conventional solid-state reaction procedure. A stochiometric mixture of $CaCO_3$, Mn_2O_3 and Pr_6O_{11} was heated and grinded several times. The solid state reaction was controlled by X-ray diffraction. After the reaction was completed, the pure-phase powder was pressed and sintered to pellets with a density of about 60% of the nominal density.

The PCMO thin films were grown on single-crystalline $SrTiO_3$(STO) (001) and MgO (001) substrates by PLD. The deposition was performed at a background oxygen pressure of $p = 0.2$ mbar with a substrate temperature of $T = 720$ °C and an energy density of the laser beam of $E = 1.5$ J/cm^2.

The epitaxial films are c-axis oriented and exhibit a 45° twist-epitaxial relation with respect to the substrate. The lattice parameters of the samples are summarized in Table 1. Compared to the single crystalline values, the as prepared films reveal an elongated c-axis. Whereas the lattice mismatch to both types of substrates should generate a tensile in-plane strain, i.e. a contraction of the c-axis, films grown by PLD usually show significant compressive in-plane and an elongated c-axis due to growth defects induced by the high kinetic energy of the impinging particles of the plasma plume. Furthermore, we cannot rule out that the as-prepared films exhibit an oxygen deficiency.

For the transport measurements, two sets of samples are used: (i) as prepared films and (ii) a set of samples which were additionally annealed at $T = 1060$ °C for 12 h in air. After the annealing, the full width at half maximum (FWHM) of the in-plane texture decreased from typically 0.77° to 0.63°; for the out-of-plane texture from 0.53° to 0.39°. The lattice constant also slightly changed (see Tab. 1). EDX-measurements verified that all grown films have the same composition as the used target.

Two gold-pads (distance 1 mm) were evaporated on the samples surface in order to contact the sample to the resistance measurement setup. To exclude the influence of the contact resistance and Schottky capacities on the IM transition, two- and four-probe measurements were performed on one sample at room temperature and well below the IM-transition. Within experimental errors the measured resistance in both measurement modes did not vary. Since the contact resistance therefore can be disregarded, we restricted all transport measurements to two-contact configuration for all other samples. They were performed using a Keithley 617 with an impedance of $2 \times 10^{15} \Omega$ and a sensitivity to currents down to 10^{-12} A. The measurements in magnetic fields up to 10 T were performed in a commercial Oxford-^{4}He-cryostate with superconducting magnets.

3 Results

In the following, the temperature dependence of the resistivity $\rho(T)$ of the PCMO films in variable magnetic and electric fields are presented. If not noted otherwise, all measurements are performed on an annealed 250 nm thick film on a STO (001) substrate (sample B).

Figure 1a shows a series of resistivity $\rho(T)$ curves determined in zero- and constant applied magnetic field with a constant applied voltage of 1V. External magnetic fields of different magnitudes were applied perpendicular to the film surface at room temperature, and, then, the sample was cooled down to $T \approx 30$ K. We first focus on zero-magnetic field, where the sample shows the temperature characteristics of an insulator. The measurement was stopped after reaching the measurement limit of the used instruments. A $\ln R(T)$ over T^{-1} plot Figure 1b allows an analysis of the zero-field resistivity and a comparison with two basic models: The thermally activated conduction (TAC) of small polarons [40,41] with

$$\rho(T) = \rho_0 T \exp\left(\frac{T_0}{T}\right) \tag{1}$$

and the resistance change due to variable range hopping (VRH) [39,41] with

$$\rho(T) = \rho_\infty \exp\left(\frac{T_0}{T}\right)^{0.25}. \tag{2}$$

Compared to VRH, TAC gives a much better fit in the temperature range of $100 \leq T \leq 300$ K above the magnetic ordering temperatures. The obtained fit parameters are summarized in Table 2.

3.1 Insulator-metal-transition in magnetic fields

Applying a magnetic field $\mu_0 H_{ex} > 5$T, the resistance behaviour starts to significantly deviate from the zero-field cooled case: the resistivity exhibits a magnetic-field dependent maximum, defining the transition temperature

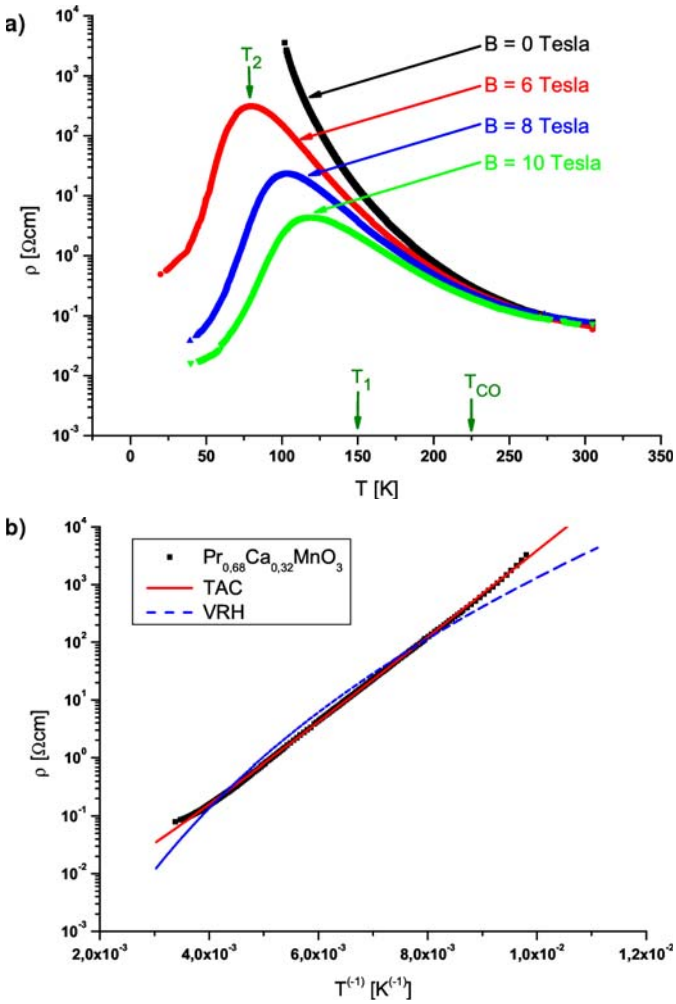

Fig. 1. (a) Temperature dependences of the resistivity of a post-annealed PCMO film on STO (001) (sample B) in different applied magnetic fields. The direction of the field was perpendicular to the sample surface. All curves are recorded for field-cooling. (b) Analysis of the zero-field electric resistivity in the temperature interval 100 K $\leq T \leq$ 300 K, measured at a constant voltage of $U = 1$ V. The $\ln R(T)$ over T^{-1} plot is compared with the models of thermally activated conduction (TAC) of polarons and variable range hopping (VRH). Obtained fit parameters are summarized in Table 2.

Table 2. Obtained fit parameters for equations (1) and (2) applied to the zero-magnetic-field, low-electric-field ($E = 5 \times 10^3$ V/m) resistivity data for $100 \leq T \leq 300$ K. PCMO film on STO (001), sample B.

	ρ_0, ρ_∞	T_0
TAC	0.18 ± 0.01 $\mu\Omega$cm K^{-1}	1857 ± 1 K
VRH	$(1.28 \pm 0.1) \times 10^{-13}m\Omega$ cm	$(3.34 \pm 0.03) \times 10^8$ K

for the magnetic-field-induced IM transition $T_2(\mu_0 H_{ex})$. Proceeding to lower temperatures the resistivity decreases. The insulating behaviour observed at higher temperatures changes to a conducting behaviour at lower temperatures (Fig. 1a). At $T \leq 120$ K, the applied magnetic field induces an IM-transition with a ρ drop of up to ten orders of magnitude.

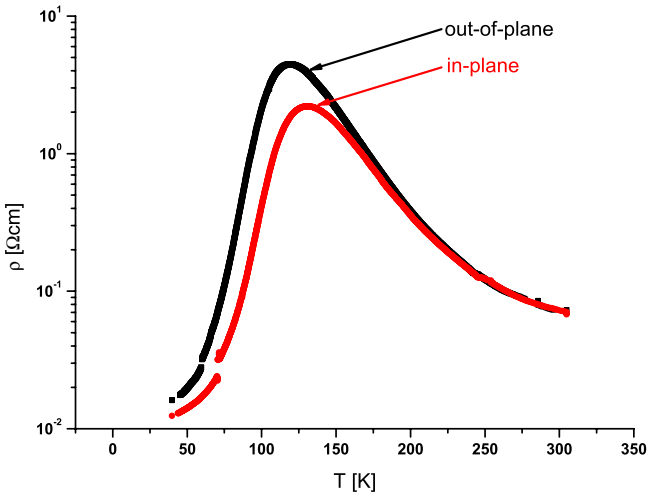

Fig. 2. Temperature dependence of the resistivity of a PCMO film on STO (001) (sample B) in a magnetic field of $\mu_0 H_{ex} = 10$ T parallel and perpendicular to the sample surface. Both curves are field-cooled measurements of the same film.

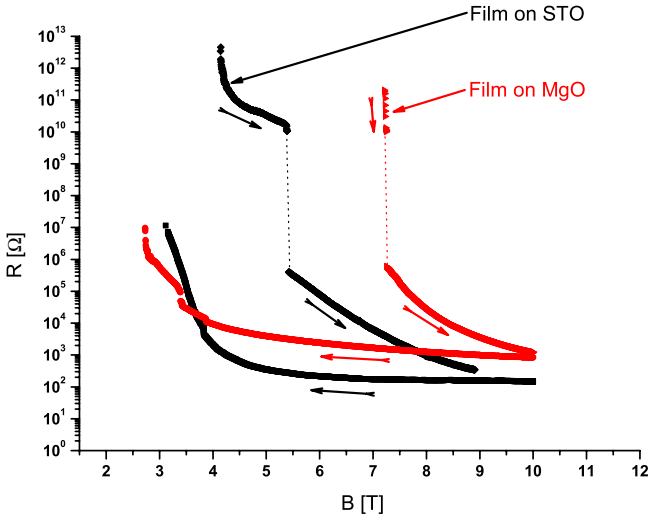

Fig. 3. Resistivity versus magnetic field of film samples on STO and MgO substrates (samples B and D) at a constant temperature of $T = 55$ K.

The influence of the orientation of the magnetic field with respect to the PCMO film plane is shown in Figure 2 for $\mu_0 H_{ex} = 10$ T. For both directions parallel and perpendicular to the film plane, the resistivity curves are very similar. However, below the transition temperature, the resistivity for the in-plane field orientation is almost half an order of magnitude smaller than for the out-of-plane orientation. Demagnetization effects seems to be not responsible for the observed difference, since the demagnetization field is with $\mu_0 H_{ex} \approx 1.5$ T much smaller than the applied field of $\mu_0 H_{ex} = 10$ T. We performed additional field dependent magnetization measurements at $T = 90$ K (not shown) which reveal that the magnetization saturates at $\mu_0 M_s \approx 1.5$ T for $\mu_0 H_{ex} \geq 6$ T. We therefore assume that the observed anisotropy of ρ is of intrinsic nature.

In Figure 3, the resistivity as a function of the applied magnetic field is presented at a temperature of $T = 55$ K. On both types of substrates, the films exhibit a large hysteresis width of around 3 T. For increasing magnetic field, the resistance shows sudden, discontinuous jumps of several orders of magnitude. These features are observed for all measured samples, however, the hysteresis width and the field values for jumps varies from sample to sample. We come back to these observations in Section 4.

3.2 Insulator-metal-transition in electric fields

The IM-transition in electric fields is investigated in two contact configuration using two different measurement modes:

(i) The temperature dependence of the resistivity was investigated in constant-current mode, to avoid an exorbitant increase of the current during the IM-transition and related strong Joule heating [44]. The measurement at constant current has, however, the consequence that the applied electric field varies with the resistance of the sample.

(ii) In addition, time dependent measurements of the resistivity in a constant electric field have been performed at constant temperature. After switching the IM-transition, the measurement was interrupted before Joule heating becomes significant.

Figure 4 shows the temperature dependence of a) the resistivity at different constant currents and b) the electric field, required to sustain these currents. After each field-cooling cycle, the sample was heated up to room temperature to recover the initial state. At the smallest current of 0.1 mA, the sample remains in a highly insulating state. With increasing current, the resistivity is systematically reduced up to three orders of magnitude at low temperatures, but the linear temperature dependence of a metal-like state is not observed.

We should note here that the crossover to the low resistivity state is related to a history-dependent critical electric field. At a fixed temperature, the first switching to the low-resistivity state requires an electric field, which is typically a factor of three higher than for adjacent switching processes (see Fig. 5). Moreover, the switching takes only place, if a moderate field of about 100 kV/m is applied within the critical temperature window between 130 K and 250 K. Samples cooled down in zero or low fields to 35 K reveal no transition, although fields up to 1000 kV/m were applied at this temperature. This history dependence is clearly visible in Figure 4b: At a temperature above 200 K the electric field increases systematically with the supplied current. At temperatures below 130 K, the fields for small currents ($I = 0.1/1$ mA) exceed those for higher currents ($I = 5/10$ mA), but, without switching the sample to a low resistivity state. Therefore, the transition at low temperatures is enabled by sufficiently high electric fields, applied above 200 K.

In Figure 5 the time dependence of $\rho(t)$ is shown at a fixed temperature of $T = 175$ K for different applied

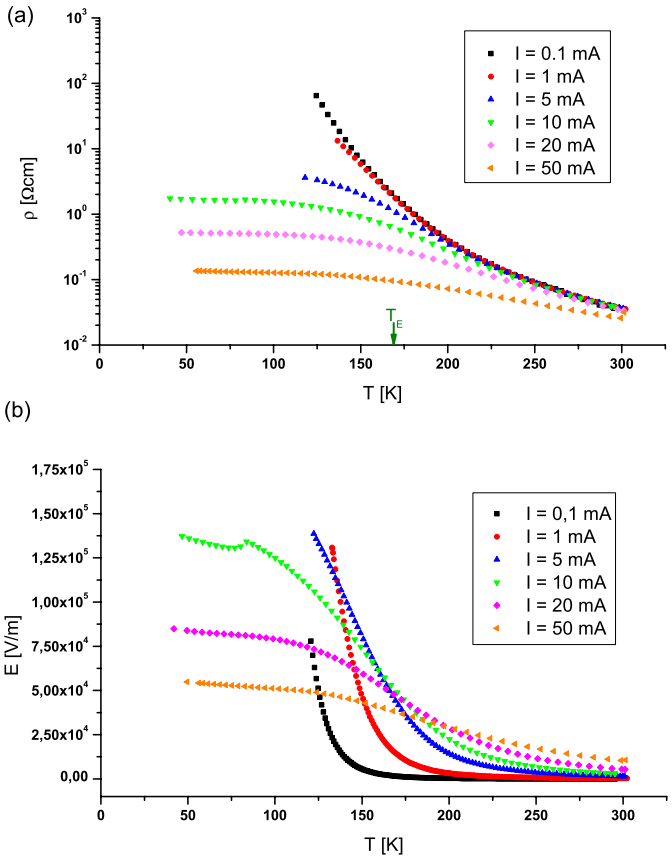

Fig. 4. (a) Temperature dependence of the resistivity of PCMO on STO (001) (sample B) in constant current mode. The resistivity is measured during field cooling in an electric field. (b) Applied external electric field to sustain the flowing currents for the same measurements shown in (a).

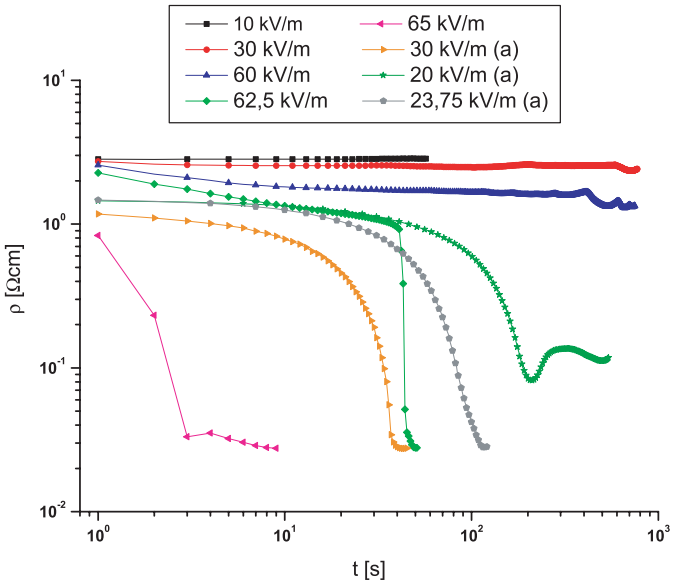

Fig. 5. Time evolution of the resistivity of PCMO on STO (sample A) at a constant temperature of 175 K. The sample was cooled down in zero-field and the measurements as a function of time were started simultaneously with applying a constant electric field. The sample was not heated up between each measurement, but a time of about 1h was passed between each step. At fields larger than 60 kV/m the measurements are stopped after the current limit (set to 140 mA) was reached. The curves named by "(a)" are obtained after application of the maximum E of 65 kV/m.

electric fields. The relaxation of the field-induced resistivity reveals two steps. A first fast step, which is beyond the time resolution of our device (100 ms) and a second one on a time scale of seconds up to minutes, strongly depending on the applied field. More precisely, the long-term relaxation is only observed within 1000 s, if the applied field is higher than 60 kV/m. The drop down of $\rho(t)$ results in an asymptotic saturation towards a low ρ value determined by the current limiter in our measurement set-up which was set to a maximum current of 140 mA. Note that after heating up to room temperature, the initial behaviour of the sample can be restored. No strong differences in the time-dependence of $\rho(t)$ are observed for our samples A-D.

The combined experiments of Figures 4 and 5 show that in the temperature window between 130 K and 250 K there is a critical switching field of around $E_c \approx (0.5\text{–}1) \times 10^5$ V/m.

In order to show microstructural influences on the resistivity behaviour and the IM-transition, Figure 6 compares as-prepared and annealed PCMO films on STO (001) and MgO (001) substrates (samples A-D). All samples show pronounced hysteretic characteristics, which differ for different substrates and are changed due to the heat treatment. The smallest hysteresis (in width and amplitude) is observed for annealed PCMO films of STO (001), having lattice parameters closest to the single crystal values.

4 Discussion

Our experiments give several indications that the IM-transition both in magnetic and in electric fields is an inhomogeneous process. Figure 7 shows a comparison of the field-cooled magnetization $M(T)$ at $\mu_0 H_{ex} = 6$ T with a field-cooled $\rho(T)$ curve for sample A. Decreasing the temperature from room temperature, the $M(T)$ curve slightly increases, however, without any characteristic feature at the nominal CO/OO temperature $T_{CO} \approx 230$ K [21]. At $T_1 \approx 150$ K, $M(T)$ exhibits a strong, escalating increase. T_1 is close to the Curie temperature of the FM state for $0.1 \leq x \leq 0.3$ reported by Jirak et al. [20]. We observe that the strong increase of $M(T)$ at T_1 is not directly related to the change of the $\rho(T)$ behaviour. The transition to a metal-like temperature characteristic sets in at $T_2 \approx 90$ K, i.e. well below T_1. This finding can be simply explained, assuming a phase separation into a conducting FM and an insulating CO/OO state at $x = 0.32$ and $T \leq T_1$. Increasing the magnetic field enlarges the volume fraction of

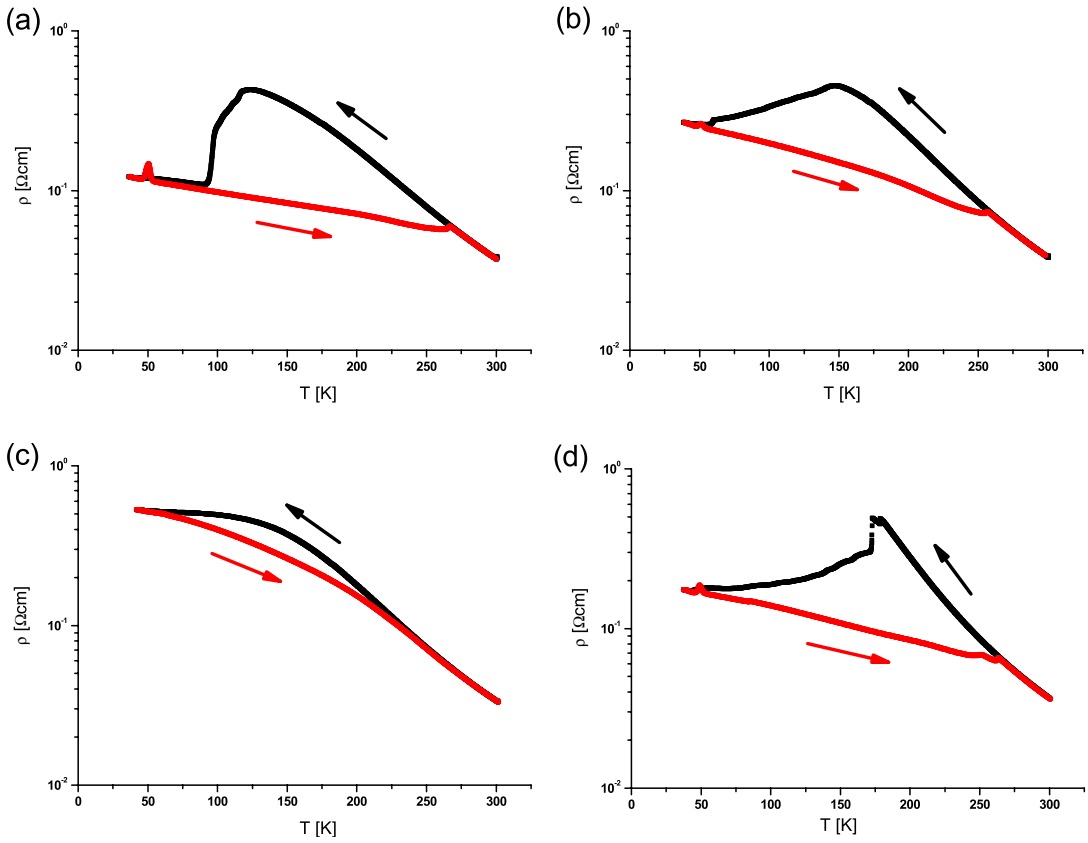

Fig. 6. Resistivity as a function of temperature in constant-current mode for PCMO films on STO and MgO before and after annealing in an applied constant current of $I = 20$ mA. (a) as-prepared film on STO (sample A), (b) as-prepared film on MgO (sample C), (c) post-annealed film on STO (sample B), (d) post-annealed film on MgO (sample D).

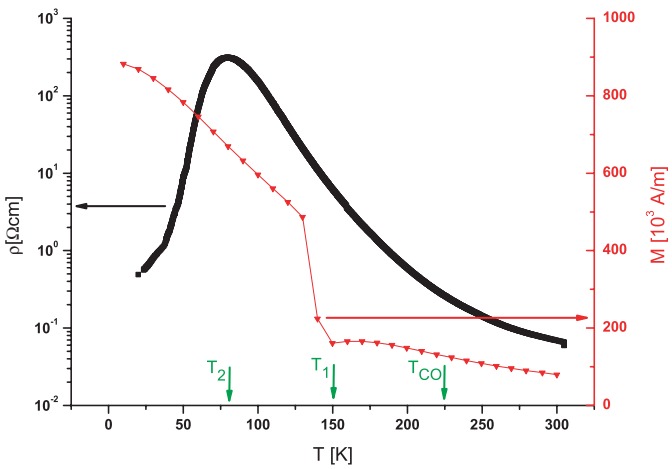

Fig. 7. Comparison of the temperature dependence of resistivity and magnetization during field cooling of the annealed PCMO film on STO (sample B). The applied field is $\mu_0 H_{ex} = 6T$ and $\mu_0 H_{ex} = 5T$ for $\rho(T)$ and $M(T)$, respectively. T_{CO} mark the OO/CO temperature according to the literature; T_1 and T_2 are defined in the text.

the conducting phase. This results in a percolation transition, where the conductive percolation path is formed after a significant growth of the FM conducting domains at $T = T_2$ (Fig. 8).

One should keep in mind that the pronounced hysteretic effects, both in electric and magnetic fields, are in accordance with a two phase model. Hysteresis is typically observed in first order transitions, where a new phase develops by nucleation and growth. The growth of the domains might be hindered by pinning at microstructural defects, which leads to hysteretic characteristics, varying from sample to sample due to minor differences in preparation. Indeed, the role of defects in the IM-transition seems to be evident. Additional heat treatments at temperatures well above the deposition temperature are necessary to enable a magnetic field induced transition in the range up to the maximum available field of 10 T. Furthermore, as prepared, the thin film samples reveal a c lattice parameter, which is slightly higher than the single crystal value. Stress reduction, healing of PLD related growth defects and oxygenation might be responsible that a post-annealing of the films is necessary to enable the IM transition in magnetic fields. Comparing Table 1, Figures 3 and 6, we observe a clear trend that lowering the c lattice parameter towards its bulk value and decreasing the width of rocking curves narrows the hysteretic width. This is most pronounced for the heat-treated sample on STO, revealing well defined and small hysteretic curves. It is out of the scope of this article to discuss in detail the role of defects on hysteretic properties, nevertheless, we find clear evidences that pinning at lattice defects plays an important role.

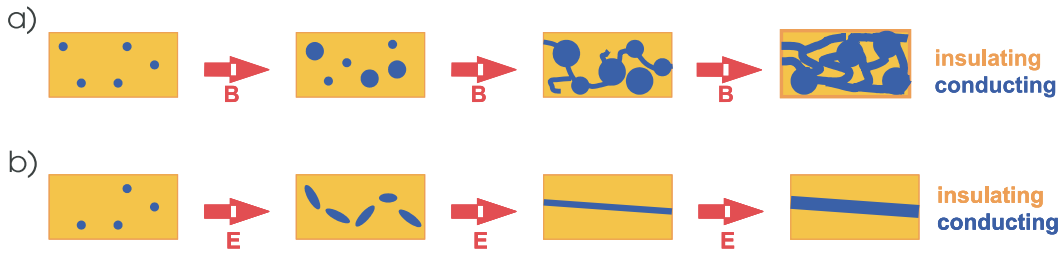

Fig. 8. Sketch of the IM-transition in a model of electronic phase-separation. (a) Magnetic field induced transition: A perpendicular applied magnetic field induces an isotropic nucleation and growth of FM clusters in the film plane leading to the formation of random conducting percolation pathes. (b) Electric field or current induced transition: The applied electric field or current causes a directed growth of conducting areas leading to the formation of one or several conducting filaments.

However, although the transitions in magnetic and electric fields show similarities, they clearly differ in the relevant temperature range. Hysteretic behaviour of the resistivity is observed between 30 K and 130 K in magnetic fields, whereas the hysteresis in electric fields is present between 50 K and 270 K, i.e. almost up to room temperature (see Fig. 6). We, therefore, suggest the existence of a second two-phase region, extended along the temperature axis of the phase diagram, in which a competition between an insulating OO/CO phase and a conducting orbital or charge disordered phase governs the IM-transition in electric fields. The first two phase region between 4 K and 130 K could be ruled by magnetic interactions and may be characterized by a competition between FM areas with a metal-like temperature dependence of the resistivity and AFM areas with OO/CO. In contrast, the second two phase region seems to be ruled by the electron-phonon interaction and reveals a competition between orbital ordering due to the cooperative static Jahn-Teller effect and orbital disordered stage with higher polaron mobility. The good fit of the TAC model to zero-magnetic-field low-electric-field resistivity data in Figure 1b supports this picture. It confirms the importance of the electron-lattice interaction in this temperature region, i.e. the electric conduction is mediated by the activated motion of JT polarons which is in agreement with [41]. Moreover, the absence of a significant anomaly in the $R(T)$ behaviour indicates the absence of a sharp OO/CO ordering temperature on a macroscopic scale and supports the idea of a smooth $R(T)$ change by the continuous change of the polaron- and orbital-ordered volume fraction.

The sketches in Figure 8 summarize the main consequences of the two phase model for both fields. At sufficiently low temperatures (below T_1), conducting FM domains are formed which enlarges with decreasing temperature and/or increasing magnetic field and the IM-transition is defined by the percolative threshold. Since, at a fixed temperature and field, the resistivity is lower if the field is applied in the film plane (Fig. 2), we expect a preferred growth of the domains in the field direction and an almost isotropic perpendicular extension. However, above the percolation threshold, the resistivity decreases systematically with the temperature due to the increasing volume fraction of the conductive phase (Fig. 8a).

In principle, a percolative transition is also expected in an electric field (Fig. 8b). However, above the percolative threshold, the resistivity tends to increase with decreasing temperature and the samples reveal a non-unique relation between current and electric field (Fig. 4). Therefore, the current-carrying cross section might be determined by the supplied current or the electric field. For such an electrically driven phase transition, an anisotropic elongation of the conductive domains parallel to the local field (or the current) is expected, which leads to the formation of a conduction filament, similar to the photon supported field-induced transition [14]. One should note that an increasing volume fraction of the conductive phase will strongly increase the local electric fields in the remaining insulating areas, because it is mainly sustained by the insulating phase and shunted in the low-resistivity phase. In contrast to the magnetically induced IM transition, the local driving force is therefore strongly modified by the spatial pattern of insulating and conducting domains. Thus, we expect a directed growth of the conducting phase with a tendency to build up filaments. Locally developing strong field maxima might be responsible for the escalating or avalanching changes in the resistivity (Figs. 4–6).

As we have mentioned in the introduction, it is still unclear which type of ordering, orbital and/or charge, is relevant for the electrically induced transition. It has been theoretically predicted, that melting of a CO state requires an electrical field $E_c = 10^7$ V/m [43]. This is two orders of magnitude higher than the experimentally observed switching field of about 10^5 V/m. The discrepancy tends to support the picture of electronic phase separation: in this state the local field in the insulating phase is much stronger than the experimentally observed averaged field. For a pure OO state, one may consider a disordering mechanism by electric current driven displacements of static JT polarons, followed by an onset of polaron motion. The observed E_c corresponds to a potential energy of about 2 meV per polaron, which is much smaller than the Jahn Teller distortion energy of 250 meV [45] and also smaller than the energy scale of the thermal phase

transition at T_{CO} (≈20 meV). Our observation, that the electric field or current induced IM-transition is enabled by sufficient large currents or fields above 200 K might give rise to the speculation that the cooperative static ordering of JT polarons (forming an highly insulating state) can be suppressed to some extend or in some regions by the flowing polaron currents.

Although we cannot determine CO or OO as the relevant mechanism of the IM-transition in electric fields from the related energy scales, the observed two time scales involved in the relaxation of the resistivity (Fig. 5) give another strong hint: The short one might be attributed to pure electronic effects such as CO, whereas the long-term relaxation is probably related to small atomic displacements in the MnO_6 octahedron which gives rise to orbital ordering. Since the latter is only observed for strong electric fields sufficient to induce a low-resistivity state, we expect the disordering of an OO ground state to be responsible for the electrically induced IM-transition. Consistent to the competing orders of the second two-phase region suggested above, the low resistance behaviour above the percolation threshold is then still dominated by an activated polaron transport in contrast to the more 'metal'-like behaviour of the induced conducting phase in a magnetic field. These issues will be worked out in more detail in a forthcoming contribution.

5 Summary

The IM-transition in both, magnetic and electric fields reveals a pronounced hysteretic characteristic. Most of the experimental results can be coherently explained in terms of a phase separation model, in which the volume fraction of the conductive phase increases with the driving force, i.e. the IM-transition is a percolative transition. The domain seems to grow preferentially along the applied fields. In case of an applied electric field, the reaction of a spatially inhomogeneous conductivity on the electric field distribution might explain some avalanche-like temporal behaviour of the resistance. The shape and the width of the hysteretic resistivity depend on the substrate material and subsequent heat treatments, indicating that pinning effects of the growing domains at materials defects and preparation-caused strains have to be taken into account. This is indeed one main cause of the variability of the IM-transitions in different films.

However, the phases which are involved in the IM-transition are different for both fields. In magnetic fields, the transition takes place at temperatures below the Curie temperature of about 150 K and the competing phases are a conducting FM and an insulating OO/CO AFM phase. An electrically driven transition is only observed, if the electric field is applied in a temperature range from the ordering temperature $T = 250$ K down to 130 K, where a competition between an OO/CO and orbital/charge disordered state is expected. In contrast to the IM-transition in magnetic fields, the volume fraction of the conducting phase doesn't increase with decreasing temperature, i.e. the transition should be only expected as field or current-driven. From our relaxation experiments we conclude, that the mobilization of polarons due to the disappearance of Jahn-Teller orbital ordering is responsible for the electrically induced low-resistivity state. If both different two phase regions overlap or not cannot be evaluated from our experiments.

This work is supported by the Deutsche Forschungsgemeinschaft (DFG) and by the SFB 602. We acknowledge valuable discussions with P. Moschkau, B. Damschke, V. Moshneaga and K. Samwer.

References

1. Y. Tomioka, A. Asamitsu, H. Kuwahara, Y. Moritomo, Phys. Rev. B **53**, R1689 (1996)
2. Y. Tomioka, A. Asamitsu, Y. Moritomo, J. Phys. Soc. Jpn. **64**, 3626 (1995)
3. M.R. Lees, J. Barratt, G. Balakrishnan, D. McK. Paul, Phys. Rev. B **52**, R14303 (1995)
4. H. Yoshizawa, H. Kawano, Y. Tomoika, Y. Tokura, Phys. Rev. B **52**, R13145 (1995)
5. H. Yoshizawa, H. Kawano, Y. Tomioka, Y. Tokura, J. Phys. Soc. Jpn. **65**, 1043-1052 (1996)
6. A. Anane, J.-P. Renard, L. Reversat, C. Dupas, P. Veillet, M. Viret, L. Pinsard, A. Revcolevschi, Phys. Rev. B **59**, 77 (1999)
7. A. Asamitsu, Y. Tomioka, H. Kuwahara, Y. Tokura, Nature **388**, 50 (1997)
8. V. Ponnambalam, S. Parashar, A.R. Raju, C.N.R. Rao, Appl. Phys. Lett. **74**, 206 (1999)
9. S. Parashar, E.E. Ebenso, A.R. Raju, C.N.R. Rao, Sol. Stat. Comm. **114**, 295 (2000)
10. S. Parashar, L. Sudheendra, A.R. Raju, C.N.R. Rao, J. Appl. Phys. **95**, 2181 (2004)
11. J. Stankiewisz, J. Sese, J. Garcia, J. Blasco, C. Rillo, Phys. Rev. B **61**, 11236 (2000)
12. Y. Morimoto, H. Kuwahara, Y. Tomioka, Y. Tokura, Phys. Rev. B **55**, 7549 (1997)
13. V. Kiryukhin, D. Casa, J.P. Hill, B. Keimer, A. Vigliante, Y. Tomioka, Y. Tokura, Nature **386**, 813 (1997)
14. M. Fiebig, K. Miyano, Y. Tomioka, Y. Tokura, Science **280**, 1925 (1998)
15. T. Mori, K. Ogawa, K. Yoshida, K. Miyano, Y. Tomioka, Y. Tokura, J. Phys. Soc. Jpn. **66**, 3570 (1997)
16. K. Miyano, T. Tanaka, Y. Tomioka, Y. Tokura, Phys. Rev. Lett. **78**, 4257 (1997)
17. K. Ogawa, W. Wei, K. Miyano, Y. Tomioka, Y. Tokura, Phys. Rev. B **57**, R15033 (1998)
18. M. Fiebig, K. Miyano, Y. Tomioka, Y. Tokura, Appl. Phys. Lett. **74**, 2310 (1999)
19. D. Casa, V. Kiryukhin, O.A. Saleh, B. Keimer, J.P. Hill, Y. Tomioka, Y. Tokura, Europhys. Lett. **47**, 90 (1999)
20. Z. Jirak, S. Krupicka, Z. Simsa, M. Dlouha, S. Vratislav, J. Magn. Magn. Mater. **53**, 153 (1985)
21. T. Tonogai, T. Satoh, K. Miyano, Y. Tomioka, Y. Tokura, Phys. Rev. B **62**, 13903 (2000)

22. J.P. Hill, C.S. Nelson, M.V. Zimmermann, Y.-J. Kim, Doon Gibbs, D. Casa, B. Keimer, Y. Murakami, C. Venkataraman, T. Gog, Y. Tomioka, Y. Tokura V. Kiryukhin, T.Y. Koo, S.-W. Cheong, Appl. Phys. A **73**, 723 (2001)
23. M.V. Zimmermann, C.S. Nelson, J. P. Hill, Doon Gibbs, M. Blume, D. Casa, B. Keimer, Y. Murakami, C.-C. Kao, C. Venkataraman, T. Gog, Y. Tomioka, Y. Tokura, Phys. Rev. B **64**, 195133 (2001)
24. M.B. Salamon, M. Jaime, Rev. Mod. Phys. **73**, 583 (2001)
25. J.M.D. Coey, M. Viret, S. von Molnar, Adv. Phys. **48**, 167 (1999)
26. A. Daoud-Aladine, J. Rodriguez-Carvajal, L. Pinsard-Gaudart, M.T. Fernandez-Diaz, A. Revcolevschi, Phys. Rev. Lett. **89**, 97205 (2002)
27. V.I. Anisimov, I.S. Elfimov, M.A. Korotin, K. Terakura, Phys. Rev. B **55**, 15494 (1997)
28. D.V. Efremov, J. van den Brink, D.I. Khomskii, Nature Materials **3**, 853 (2004)
29. M. Varela, W. Luo, J. Tao, A. Franceschetti, A.R. Lupini, W. Tian, R. Jin, B.C. Sales, D.G. Mandrus, S.J. Pennycook, S.T. Pantelides, preprint
30. A. Moreo, S. Yunoki, E. Dagotto, Science **183**, 2034 (1999)
31. E. Dagotto, *Nanoscale Phase Separation and Colossal Magnetoresistance* (Springer-Verlag, Berlin, Heidelberg, New York 2003)
32. E.L. Nagaev, JETP Lett. **6**, 16 (1967)
33. M. Jaime, P. Lin, S.H. Chun, M. B. Salamon, P. Dorsey, M. Rubinstein, Phys, Rev. B **60**, 1028 (1999)
34. A. Moreo, M. Mayr, A. Feiguin, S. Yunoki, E. Dagotto, Phys. Rev. Lett. **84**, 5568 (2000)
35. M. Mayr, A. Moreno, J.A. Verges, J. Arispe, A. Feiguin, E. Dagotto, Phys. Rev. Lett. **86**, 135 (2001)
36. M. Fäth, S. Freisem, A. A. Menovsky, Y. Tomioka, J. Aarts, J.A. Mydosh, Science **285**, 1540 (1999)
37. T. Becker, C. Streng, Y. Luo, V. Moshnyaga, B. Damaschke, N. Shannon, K. Samwer, Phys. Rev. Lett. **89**, 237203 (2002)
38. M. Uehara, S. Mori, C.H. Chen, S.W. Cheong, Nature **399**, 560 (1999)
39. M.R. Lees, J. Barratt, G. Balakrishnan, D. McK. Paul, C.D. Dewhurst, J. Phys.: Cond. Mat. **8**, 2967 (1996)
40. T. Holstein, Ann. Phys. **8**, 343 (1959)
41. V.G. Prokhorov, G.G. Kaminsky, V.S. Flis, Low Temp. Phys. **25**, 792 (1999)
42. R. Fichtl, V. Tsurkan, P. Lunkenheimer, J. Hemberger, V. Fritsch, H.-A. Krug von Nidda, E.-W. Scheidt, A. Loidl, Phys. Rev. Lett. **94**, 027601 (2005)
43. R.Y. Gu, Z.D. Wang, C.S. Ting, Phys. Rev. B **67**, 153101 (2003)
44. P. Padhan, W. Prellier, Ch. Simon, R.C. Budhani, Phys. Rev. B **70**, 134403 (2004)
45. T. Hotta, E. Dagotta, Phys. Rev. B **61**, R11879 (2000)